An experimental-based model for the assessment of the mechanical properties of road pavements using ground-penetrating radar

An experimental-based model for the assessment of the mechanical properties of road pavements using ground-penetrating radar

Fabio TOSTI[1], Luca BIANCHINI CIAMPOLI[2], Fabrizio D'AMICO[2], Amir M. ALANI[1], Andrea BENEDETTO[2]

[1]School of Computing and Engineering, University of West London (UWL), St Mary's Road, Ealing, London W5 5RF, UK

e-mail: Fabio.Tosti@uwl.ac.uk (*Corresponding author); Amir.Alani@uwl.ac.uk

[2]Department of Engineering, Roma Tre University, Via Vito Volterra 62, 00146, Rome, Italy

e-mail: luca.bianchiniciampoli@uniroma3.it; fabrizio.damico@uniroma3.it; andrea.benedetto@uniroma3.it.

ABSTRACT

This work proposes an experimental-based model for the assessment of the stiffness of a road flexible pavement using ground-penetrating radar (GPR – 2 GHz horn antenna) and light falling weight deflectometer (LFWD) non-destructive testing (NDT) methods. It is known that the identification of early decay and loss of bearing capacity is a major challenge for effective roads maintenance and the implementation of pavement management systems (PMS). To this effect, a time-efficient methodology based on quantitative and qualitative modelling of road stiffness is developed. The viability of using a GPR system in combination with LFWD equipment is also proven.

Keywords: ground-penetrating radar (GPR); light falling weight deflectometer (LFWD); non-destructive testing (NDT); road flexible pavements; road stiffness; health monitoring and assessment; time-efficient methodology; quantitative and qualitative modelling; pavement management system (PMS).

1. INTRODUCTION

Reducing the number of accidents is a major priority and a challenging target to achieve for road administrators. Accidents are generally related to geometric issues [1] and unfavourable serviceability conditions [2]. Firstly, improper design of road geometric elements affects drivers' perception of the road trajectory. Secondly, low road serviceability levels lead, above all, to lack of friction between the vehicles and the road surface. With regard to the latter issue, the intercorrelation between pavement decay and frequency of accidents is well known [3]. To this effect, an extensive and time-efficient assessment of roads at the network level is crucial for road administrators and agencies to define priorities of intervention and decrease the likelihood of envisaged accidents.

Most of the damages in flexible pavements occur where the stiffness of the asphalt and load-bearing layers is low. Therefore, an effective assessment of the strength and deformation properties of these layers can lead to identifying causes and locating the depth of damages. In addition, a prompt detection of early decay and loss of bearing capacity represents the real challenge to tackle for road administrators.

It is known that the bearing capacity of subgrade soils can be evaluated by on-site [4, 5] and laboratory [6] tests. These mainly assess the deformation of the pavement when a constant stress is applied. Due to the high operational time and costs, these tests are usually carried out on a few road sections and provide only partial information on the stiffness of the layers. Furthermore, these methods are intrusive and require to close the highway entirely or partially, with implications for the driving safety of roads.

In view of the above limitations, non-destructive testing (NDT) methods have become popular for the assessment of the mechanical properties of pavements. Falling weight deflectometer (FWD) [7] and light falling weight deflectometer (LFWD) [8, 9] are widely used for the investigation of integrated flexible pavement structures and for construction quality control of unbound materials, respectively. Nevertheless, LFWD has found also effective application in the assessment of stiffness

of bound layers [10, 11]. The FWD method relies on the measurement of deflections produced by a known falling mass loading the pavement surface. The main limitation of this method is that data can be collected only at discrete points, thereby affecting time and cost of the operations. To fill this gap, fully equipped non-destructive testing lorries for estimation of pavement strength and deformation properties at traffic speed have been therefore developed. In this regard, the curviameter [12] uses geophones to measure the velocity of vertical displacements of the pavement under the passage of the rear axle of the truck. Collection velocity is 18 km/h. The deflection bowl is obtained by integration of the measurements from the geophones, which are placed in a chain system. The main limitation of this equipment relates with the integration process. In this regard, an accurate calibration of the geophones is required. Furthermore, the need to respect a constant speed and the impossibility to make measurements in curves with radius lower than 40m are worthy of mention. A traffic speed deflectometer (TSD) [13] is another moving deflectometer. It operates at speeds up to 90 km/h and it is equipped with a long and rigid beam placed inside a semi-truck. A dedicated dead weight of 100 kN is located in the proximity of the rear axle. High-rate sensors, including Doppler sensors, accelerometers and laser distance sensors, ensure that vertical pavement deflection velocities are recorded. Deflection velocities divided by the instantaneous vehicle speed produce the deflection slopes at discrete points along the TSD route. Several internal and external factors may affect the accuracy and precision of TSD measurements. These include calibration and quality assurance procedures, wind and temperature during the measurement, pavement roughness and tire-pavement interaction [14]. Although all the aforementioned methods are reliable and time-efficient, estimation of the strength and deformation properties of pavement layers requires a multi-stage collection of complementary information from different equipment (e.g., ground-penetrating radar (GPR)). In addition, the integration of this information requires a repeat of the data collection stage for each equipment along the whole stretch of the investigated roadway.

GPR has been extensively used in highway engineering as a result of the high reliability in the assessment of the geometric properties and physical properties of the pavement layers. GPR systems equipped with air-coupled antennas and connected to vehicles are mostly used for data collection at traffic speed. The GPR working principles rely on the emission of electromagnetic (EM) waves towards the ground. The emitted waves are then reflected back from the targets (typically represented by the interfaces of the layers) and are received by a receiving antenna. The collected signal is therefore displayed and stored for data processing and interpretation purposes. To date, GPR is successfully utilised in several disciplines including civil engineering [11], demining [15], archaeology [16], geology [17], glaciology [18] and much more.

As a common practice in highway engineering, the GPR and FWD methods are used separately for the assessment of the geometric (i.e., evaluation of the layer thicknesses) and the strength and deformation properties (i.e., evaluation of the deflection bowl) of road flexible pavements, respectively. The integration of the above information allows to evaluate reliable values of stiffness modulus of the pavement layers.

In view of the aforementioned limitations and state-of-the-art practices in the assessment of the mechanical properties of flexible pavements, the development of a non-destructive testing methodology for real-time identification of early decay and loss of bearing capacity of roads at traffic speed would stand as a step forward compared with the traditional methods. Value added would be to provide an estimation of the pavement stiffness based on geometric, physical and mechanical attributes of the subsurface integrated into a unique model. This would emphasize strengths and narrow weaknesses of the above NDTs.

A first modelling approach was developed by Tosti et al. [19]. A ground-coupled GPR antenna system and LFWD equipment were used to collect a dense dataset on a flexible pavement structure. The model was based on the peak amplitudes of the GPR signals reflected at the interfaces of the road

layers and the stiffness moduli estimated using LFWD. The concept proposed by Tosti et al. [19] is here taken as a reference and it is further developed using an air-coupled GPR antenna system.

It is important to emphasize the importance of the proposed methodology in assessing early decay and loss of bearing capacity of the load bearing layers more efficiently than the state-of-the-art NDT methods. This information would be crucial for road administrators in order to create comprehensive databases of the road pavement conditions at the network level for implementation in pavement management systems (PMSs). This would allow for prioritisation of road maintenance operations, reduction of costs and a decrease in the likelihood of envisaged accidents.

The paper is outlined as follows: in Section 2, the aim and objectives are presented. The theoretical framework is discussed in Section 3. Section 4 presents the methodology, whereas the experimental design (test site and equipment) is detailed in Section 5. The ground-truth information and the preliminary data analysis are discussed in Section 6. The modelling is presented in Section 7, whereas results and discussion are reported in Section 8. Finally, the conclusion and future prospects are discussed in Section 9.

2. AIM AND OBJECTIVES

The primary aim of this project is to address a major challenge in the identification of early decay and loss of bearing capacity in road flexible pavements using GPR and LFWD. To achieve this aim, the following objectives are set:

- to develop a time-efficient methodology for estimating the stiffness of the pavement structure;
- to demonstrate the viability of using an air-coupled GPR antenna system in combination with LFWD equipment.

3. THEORETICAL FRAMEWORK

The GPR method is based on the theory of the EM fields. When an EM wave is emitted by a source, propagation is ruled by the dielectric properties of the medium that is passed through (case of non-

magnetic targets). In more detail, propagation speed and attenuation of the wave are related to the relative dielectric permittivity ε_r [-] and the electrical conductivity σ [Sm^{-1}], respectively. When a dielectric discontinuity is encountered, the radiated energy is partly reflected back to the receiving antenna and partly transmitted in depth. From the analysis of the collected signal, it is therefore possible to reconstruct the geometric features of the discontinuities.

Within this framework, the volumetric content of air and water that fills the inter-particle voids of pavement materials highly influences the dielectrics of the road pavement layers. However, compaction conditions of the pavement layers are also highly dependent on the content of inter-particle voids in construction materials. Hence, it is reasonable to assume that compaction of pavement materials may affect the EM behaviour of the layers [20]. With regards to the load-bearing layers and subgrade soils, it is also worth mentioning that soil particle compaction is highly dependent on their grain size distribution. This affects, in turn, the number of contacts between the grains and, hence, the shear strength of the material (along with the particle mineralogy and roughness) [21]. To this effect, compaction is performed on site after the laying out of loose soil granular materials. This allows to activate frictional resistance and interlocking of grains in order to reach a higher bearing capacity.

The strength of bearing soils in unsaturated conditions is also highly dependent on the physical state of water within the inter-particle voids. In this regard, it is known that free water can create differing physical-chemical bonds as a function of both size and type of soil particles. These bonds affect the cohesion between particles and, hence, the bearing capacity of subgrades. According to Mitchell [22], the dielectric properties of materials (e.g., dielectric loss and permittivity) are also dependent on the aforementioned inter-molecular bonds. Furthermore, Carpenter et al. [23] demonstrated how several pavement damages visible on the surface, such as transverse cracking, are caused by freeze-thaw cycling affecting the whole pavement structure. Indeed, this process induces a seasonal volumetric contraction and dilation of the unbound layers and, mostly, the base layer. More recently, Scullion

and Saarenketo [24] also proved the high correlation between the thermal susceptibility and the water suction in unbound bearing soils. Changes in the dielectric behaviour of soils were also found to be highly related to water suction effects.

In view of the aforementioned research, it is likely to expect a relationship between the dielectric and the strength and deformation properties of the unbound materials of road pavements [25, 26].

A road flexible pavement is generally described as a multi-layer structure composed of hot-mixed asphalt (HMA) bitumen-bound layers overlaying unbound granular courses. This structure is laid over a bearing subgrade [27]. It is known that the bond of the shallowest road layers is due to the high shear stresses transferred by the moving vehicles at the wheel-surface contact. Conversely, unbound granular materials are used for the construction of the foundation layers. These latter along with the subgrade soil receive stress generation from the above layers and bear the major structural contribution in terms of loads [28].

By considering a flexible pavement as a simplified homogenous half-space, the stress distribution with depth can be described using the theory of Boussinesq [e.g., 29] and its generalization to multi-layer configurations [30]. To this effect, the graphical solutions proposed by Forster and Ahlvin [31], clearly show that in the surroundings of a bearing area with a radius equal to 15 cm (e.g., case of a common lorry), most of the vertical stress concentrates beyond 7 cm of depth. This depth is typically out of the thickness of an HMA layer. This occurrence was also proved using numerical simulation [32]. Hence, it can be argued that loosely bound and unbound granular layers (especially the base layer) may heavily affect the mechanical behaviour of the whole road pavement structure. To this purpose, it is worth mentioning the research work of Scullion and Saarenkeeto [24]. The authors observed volumetric shrinkage caused by freezing in several base layers of different road flexible pavements. These contractions were one order of magnitude greater than shrinkage measured in the asphalt layers and were observed to cause cracking at the surface. Furthermore, structural rutting was

investigated by Oteng-Seifah and Manke [33] and Simpson et al. [34] and was related to deformations located in the base layer and the subgrade.

In view of the research studies above, it can be argued how thickness and development of the base layer may affect the bearing capacity of a whole pavement structure.

Further to the aforementioned geometric factors, it is known how the bearing capacity of flexible pavements may be highly affected by critical physical attributes [35], such as the content of clay. The upward passage of the smallest clay slurry particles from the subgrade by capillary actions lowers the strength and deformation properties of the pavement structure. To this effect, the correlation between clay content and plastic deformation of soils under load has been widely investigated in the literature [22]. From an EM standpoint, the viability of using GPR for detection of clay in dry and saturated soils has been demonstrated. As the applied EM field is affected by the presence of clay in a medium, relevant information can be estimated from the collected signal (in both the time and the frequency domain) [36, 37]. Attenuation of the EM waves is one of the most easily detectable effects related to the presence of clay in soils. In the case of dielectric materials, signal attenuation can be expressed by the propagation loss $L = \exp\{-bz\}$ [38], with b being the attenuation coefficient and z being the investigation depth. The coefficient b is highly dependent on the electric conductivity of the medium σ [Sm^{-1}]. As clayey soils are typically characterised by high values of σ (mostly in wet conditions), then clay presence can be related to greater attenuations of the EM wave. In view of this, it can be argued that the amplitude of the received GPR signals is likely affected by the upward passage of clayey slurry particles towards the shallowest layers of a road flexible pavement.

4. **METHODOLOGY**

The study focuses on the estimation of the stiffness of a road flexible pavement whereby a unique modulus for the overall pavement strength is considered. To this purpose, experimental tests are carried out using an air-coupled GPR antenna system and LFWD equipment.

198 Outliers are first filtered out from the LFWD dataset along with the relative GPR signals. A
199 parametric model is therefore developed. In this regard, LFWD data are used as ground-truth
200 measurements of pavement stiffness for modelling purposes. On the other hand, GPR data provide
201 geometric and physical attributes about the pavement structure. The model parameters are first
202 calibrated against the ~10% of data from the full dataset. A quantitative validation of the model
203 viability is therefore carried out across the full road stretch length. Based on these outcomes, a
204 qualitative approach for the estimation of the pavement stiffness is also developed.
205

206 ## 5. EXPERIMENTAL DESIGN: TEST SITE AND EQUIPMENT

207 Experimental tests are carried out in the District of Rieti, Italy. To this purpose, 1500 m of a two-lane
208 highway (one lane per direction) with a flexible pavement structure are investigated using GPR and
209 LFWD equipment. From the available design drawings of the pavement structure, the superstructure
210 is made of a 0.05-m-thick surface layer, a 0.10-m-thick bitumen-bond base layer and a 0.30-m-thick
211 subbase layer (unbound granular material).

212 With regard to the GPR equipment, the RIS Hi-Pave HR1 2000 air-coupled antenna system,
213 manufactured by IDS Georadar, is used. The system is equipped with a mono-static antenna of 2 GHz
214 central frequency, mounted behind an instrumented van. The high frequency of investigation and type
215 of antenna system allow to collect reflections of the GPR signal from the interfaces between the
216 thinner surface layers as well as to perform the investigation at traffic speed. Traces are collected
217 every 0.027 m to allow further statistical analyses about the optimal horizontal sampling resolution.

218 Tests for the collection of ground-truth data of pavement stiffness are carried out using the LFWD
219 Prima 100 manufactured by Carl Bro Pavement Consultants Kolding. The equipment is composed of
220 a circular metal plate (diameter 100 mm) loaded by a 10 kg hammer and a set of geophones that allow
221 to record the pavement deflections δ_c [μm]. The LFWD investigation points are spaced 10 m from
222 one another so that 151 points are collected along the investigated road stretch. It is worth noting that

LFWD is a less acknowledged piece of testing equipment than the FWD for the investigation of the stiffness of bound layers. Nevertheless, LFWD is used in this study for calibration and validation purposes for consistency with past research on GPR [19] and LFWD [9, 10] as well as to foster the time-efficiency of the proposed methodology.

6. GROUND-TRUTH INFORMATION AND PRELIMINARY DATA ANALYSIS

An "equipollent" modulus of stiffness $E_{MEA,x}$ at a generic position x (corresponding to a generic load point) is calculated implementing the deflections from LFWD in the Boussinesq solution [e.g., 29] as follows [39]:

$$E_{MEA,x} = \frac{k(1-\nu^2)\sigma_x R}{\delta_{c,x}} \quad (1)$$

where k is a constant equal to 2 (case of flexible pavements), ν [-] is the Poisson ratio, σ_x [MPa] is the load stress, R [mm] is the plate radius and $\delta_{c,x}$ [μm] is the deflection measured at the center of the LFWD plate. A number of 6 loading tests were performed at each survey point to ensure statistically significant data outputs [8]. Correction of the estimated stiffness due to temperature effects is not applied to the LFWD data, as the test conditions are close to the benchmark temperature suggested in the literature [40].

The use of LFWD deals satisfactorily with the model outline discussed above, as the expected maximum depth of the bottom of the base layer is, by design drawings, around 15 cm. This depth matches well the maximum depth of the deflection basin expected for this equipment in road pavement investigations [9]. From now on, values of $E_{MEA,x}$ estimated by Eq. (1) will be used as ground-truth data for modelling purposes. This parameter will be referred to as "measured stiffness modulus" $E_{MEA,x}$ at a generic position x.

Each dataset of 6 LFWD measurements collected at the 151 investigation points along the "full" road stretch length l_{tot} is processed in terms of force applied, vertical stress and deflections. Datasets with low statistical significance [9] are discarded in full and the relative investigation points are removed

from the statistical population. In view of this, the relevant LFWD investigation points are reduced from 151 to 120 so that a 1200m-long road stretch (from now on referred to as "processed road stretch" l_{proc}) is considered for modelling purposes. The related GPR traces are also consistently filtered out from the GPR dataset. A standard processing scheme for road inspections is applied to the GPR data [41]. In this regard, the zero-offset removal, the bandpass filtering and the cut-off of the air layer are applied.

7. MODELLING

7.1 Model outline

An experimental-based parametric model for the estimation of the stiffness of road flexible pavements is developed. Strength and deformation properties of a road flexible pavement at a generic position *x* are expressed, in terms of stiffness modulus $E'_{MOD,x}$ [MPa], as follows:

$$E'_{MOD,x} = \alpha\left(E_{MOD,x}\right) E_{MOD,x} \tag{2}$$

with $\alpha(E_{MOD,x})$ being a fitting function and $E_{MOD,x}$ [MPa] being a first approximation stiffness modulus. This latter parameter is defined as follows:

$$E_{MOD,x} = \tau_{b,x}\ \beta_x\ \gamma_x \tag{3}$$

where $\tau_{b,x}$ [m] accounts for the thickness of the base layer, β_x [MPa m^{-1}] is a scale factor and γ_x[-] takes into account the contribution of clay to the stiffness modulus.

The modelled stiffness modulus $E'_{MOD,x}$ in Eq. (2) is estimated through calibration of the $\alpha(E_{MOD,x})$ fitting function and the relative first approximation stiffness modulus $E_{MOD,x}$ (Eq. (3)). This latter requires in turn calibration of the β_x and γ_x parameters, whereas $\tau_{b,x}$ is a constant value taken from the trend of the base layer thickness. Calibration of the above parameters is carried out over a 100m-long distance within the 1200m-long processed road stretch l_{proc}.

7.2 Evaluation of the base layer thickness

The thickness of the base layer $\tau_{b,x}$ is assessed with reference to the two-way travel time (TWTT) distance covered by the GPR signal to pass through the concerning layer [42]. The value of this parameter at a generic position *x* is calculated as follows:

$$\tau_{b,x} = \frac{c\,\Delta t_x}{2\sqrt{\varepsilon_{r,b,x}}} \tag{4}$$

where c [ms^{-1}] is the wave velocity of propagation in the free space, Δt_x [s] is the temporal distance between the reflection amplitude peaks of the top and the bottom of the base layer (i.e., the peak-to-peak time distance), and $\varepsilon_{r,b,x}$ [-] is the relative dielectric permittivity of the material passed through within the base layer.

Fig. 1 depicts a comparison between trends of measured stiffness modulus $E_{MEA,x}$ (Fig. 1(a)) and base layer thickness $\tau_{b,x}$ (Fig. 1(b)). The similarity between the two trends in shown; hence, a correlation between these two parameters could be likely deemed.

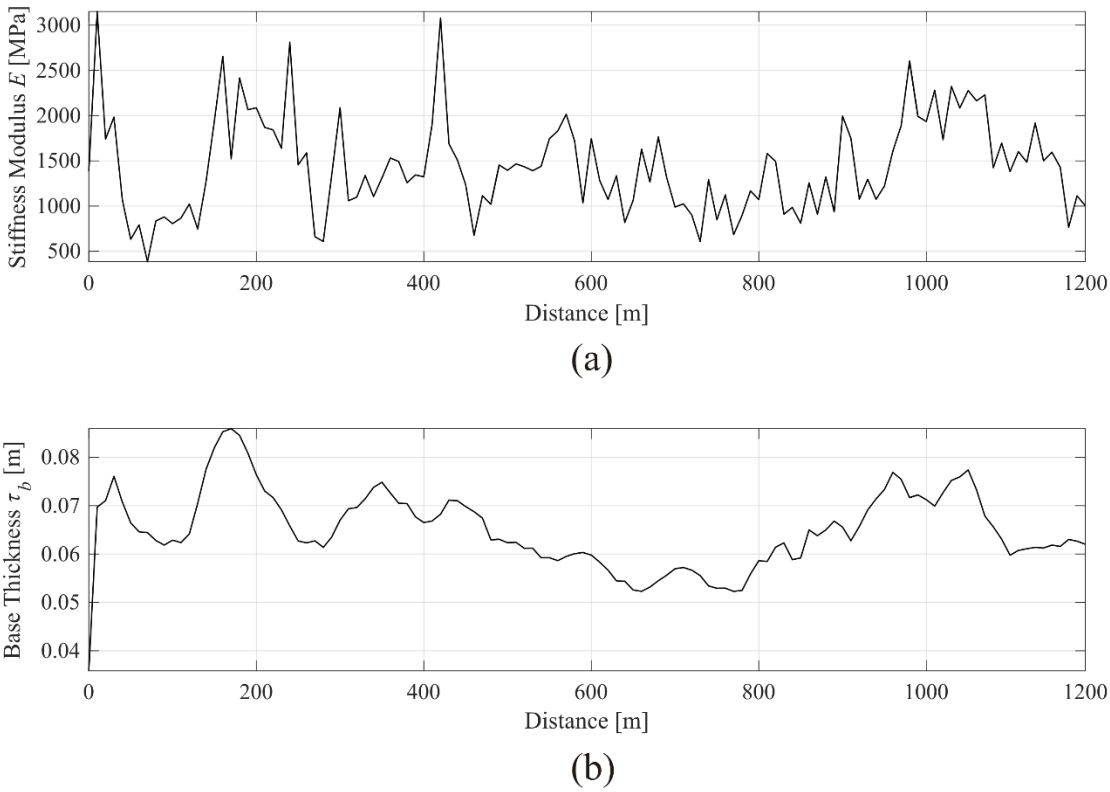

Fig. 1. Comparison between trends of (a) measured stiffness modulus (LFWD – Eq. (1)) and (b) base

286 layer thickness (GPR – Eq. (4)).

287

288 **7.3 Model calibration**

289 A 100 m-long section (l_{cal}), located between markers 170 m and 270 m of the processed road stretch
290 l_{proc}, is randomly selected for calibration purposes. This distance represents the 6.7% and the 8.3% of
291 the "full" (l_{tot} = 1500 m) and the "processed" (l_{proc} = 1200 m) road stretch lengths, respectively.

292 It is worth noting that the outcomes of the calibration process discussed hereafter are representative
293 of the specific testing conditions of this study. These include the flexible pavement structure
294 described in Section 5 and the percentage of ground-truth data of pavement stiffness taken for
295 calibration purposes. Hence, other values of the calibration parameters apply in the case of different
296 boundary conditions.

297

298 **7.3.1 Dimensional scaling**

299 The scale factor β_x is set as:

300 $$\beta_x = \frac{E_{MEA,x,MAX_{[l_{proc}]}}}{\tau_{b,x\,MAX_{[l_{cal}]}}} \quad (5)$$

301 where $E_{MEA,x,MAX_{[l_{proc}]}}$ is the maximum value of stiffness modulus estimated throughout the 120
302 investigation points within the processed distance l_{proc} = 1200 m using Eq. (1), and $\tau_{b,x,MAX}$ is the
303 maximum thickness of the base layer calculated using Eq. (4) within the randomly selected calibration
304 road stretch l_{cal}.

305 Fig. 2 shows the trend of preliminarily modelled stiffness modulus $E^*_{MOD,x} = \beta_x\,\tau_{b,x}$ along the
306 calibration road stretch. It can be seen how the preliminary application of the model generally tends
307 to overestimate the measured ground-truth data. This mismatch is further addressed in Section 7.3.3
308 using a dedicated fitting function.
309

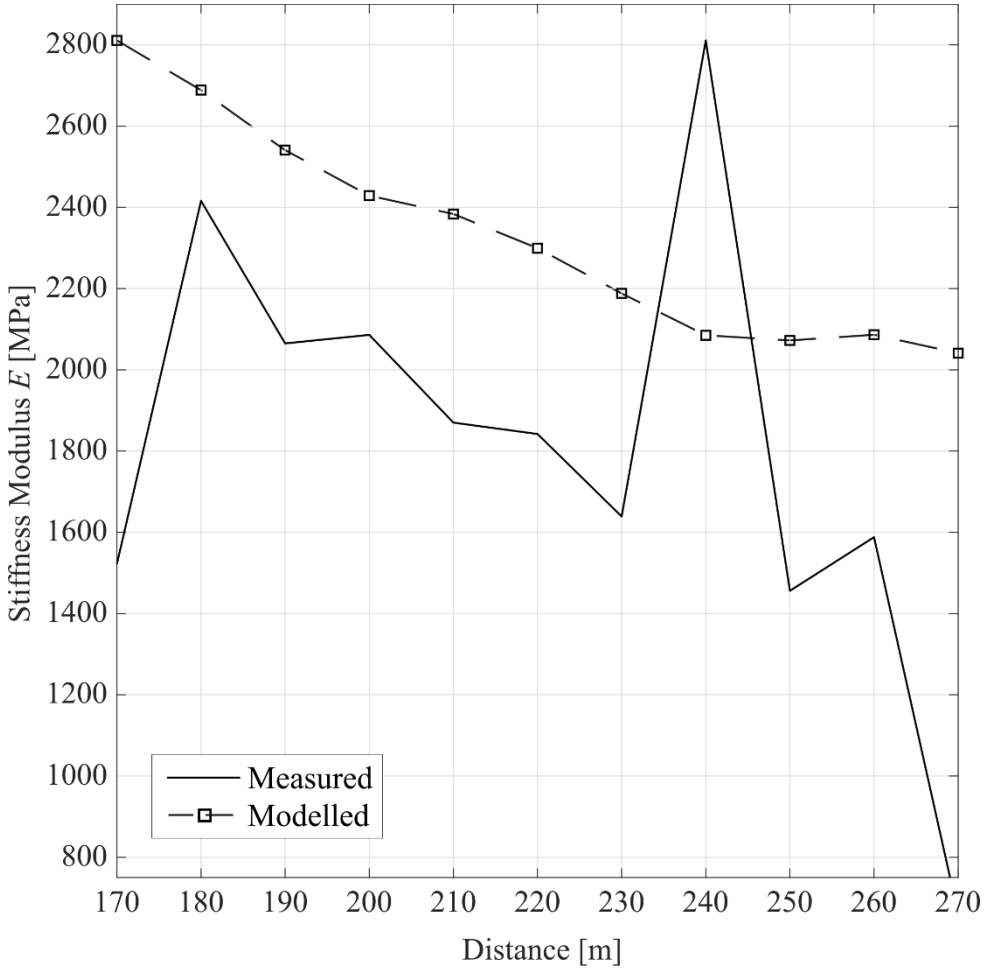

Fig. 2. Comparison between trends of measured (solid line) and preliminarily modelled (dashed line with square markers) stiffness modulus along the 100m-long calibration road stretch.

7.3.2 Clay contribution

The amplitude of the central peak of the frequency spectrum A_p is considered as the benchmark parameter to account for the presence of clay rising from the foundation level [27, 28]. To this purpose, geological maps of the site [43] are analysed and the investigated stretch of road is classified as belonging to a poorly-clayey geological area. Hence, highly attenuated frequency spectra are interpreted as indicators of likely presence of clay and are related to areas of early decay and loss of road bearing capacity. On the contrary, standard frequency spectra are interpreted as indicators of stability in terms of strength and deformation properties of the pavement.

The stair function $\gamma(A_{p,x})$ is defined from the analysis of the central peak amplitude $A_{p,x}$ of the

frequency spectrum of the GPR signal collected at a generic position x within the calibration road stretch l_{cal}. This function is developed to lower the modelled stiffness modulus when the value of $A_{p,x}$ is lower than a reference optimal threshold value (i.e., when the spectrum is attenuated). It is expressed as follows:

$$\gamma(A_{p,x}) = \begin{cases} 0.80 & if\ A_{p,x_{[l_{cal}]}^{[0,1]}} < A_t \\ 1 & \text{otherwise} \end{cases} \quad (6)$$

where $A_{p,x_{[l_{cal}]}^{[0,1]}}$ is the central peak amplitude of the frequency spectrum, normalised in the calibration range l_{cal} and A_t is the set threshold. The threshold A_t is defined after running the model for each i^{th} value $A_{t,i}$, with i ranging between 0.80 and 1 at steps of 0.01. The trend of the i^{th} values of $A_{t,i}$ in the defined range is described by the following objective function $\varphi(A_{t,i})$:

$$\varphi(A_{t,i}) = \sqrt{\frac{\sum_{x=0}^{l_{cal}} |E_{MOD,x,A_{t,i}} - E_{MEA,x}|^2}{\sum_{x=0}^{l_{cal}} E_{MOD,x,A_{t,i}}^2}} \quad (7)$$

expressing the mismatch between the modelled ($E_{MOD,x,A_{t,i}}$) and the measured ($E_{MEA,x}$) stiffness modulus. Fig. 3 shows the performance of the model with varying values of $A_{t,i}$. A minimum value of 0.034 for $\varphi(A_{t,i})$ is reached when $A_{t,i}$ is equal to *0.857*; hence, this value is taken as the optimal threshold expressing A_t.

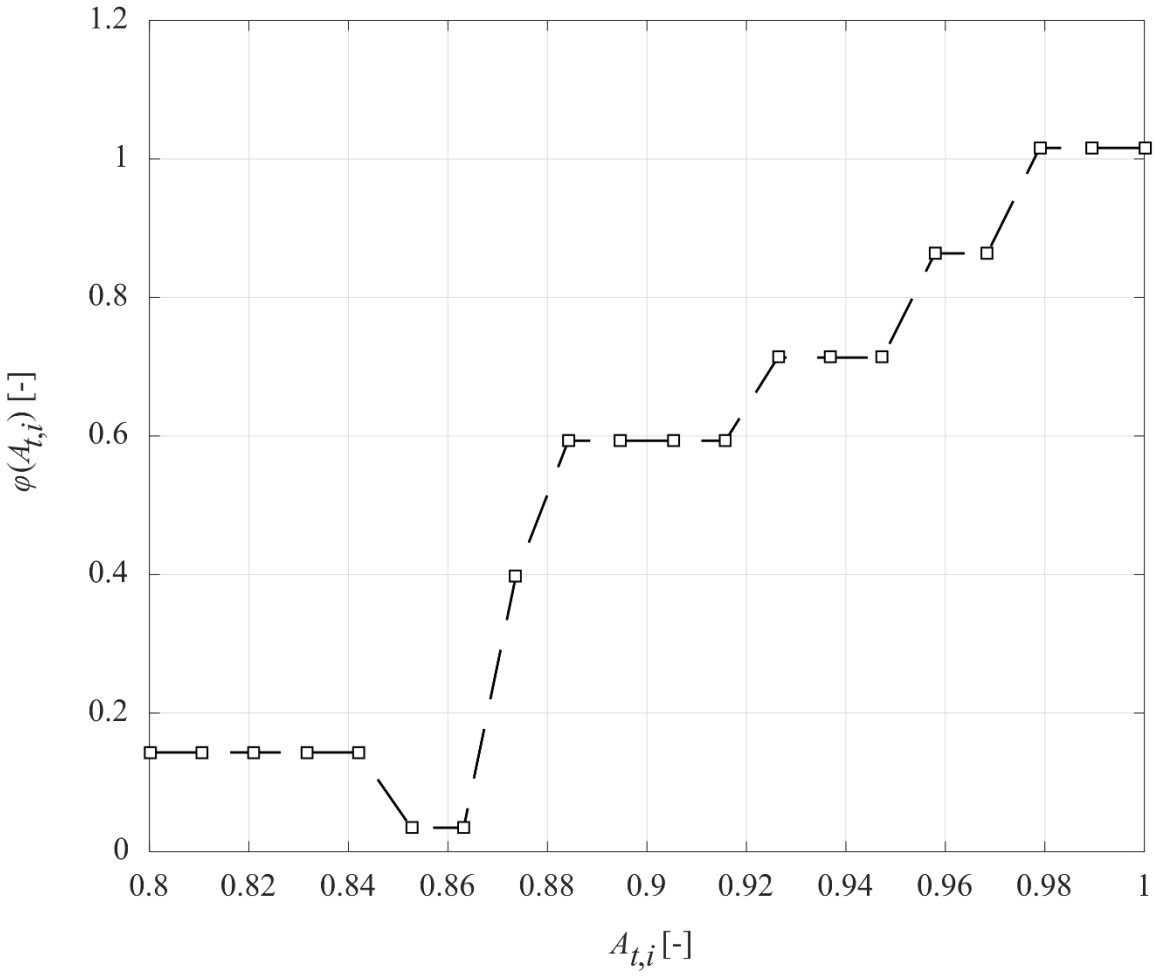

Fig. 3. The trend of the objective function $\varphi(A_{t,i})$ with varying values of $A_{t,i}$.

It is worth specifying that the $\gamma(A_{p,x})$ parameter improves the model matching at the local maximum and minimum points of the measured trend of stiffness, whereas the overall model overestimation is addressed using a dedicated fitting function, as detailed further in Section 7.3.3.

7.3.3 The fitting function

A percentile analysis of measured and modelled stiffness moduli (Fig. 4(a)) is performed to ensure accurate evaluation of the model overestimation. The ratio of the modelled to the measured percentiles (Fig. 4(b)) is therefore calculated as a reductive factor for compensation purposes. Hence, the continuous function $\alpha(E_{MOD,x})$ is derived using the following third-degree polynomial fitting

relationship:

$$\alpha(E_{MOD,x}) = \sum_{i=0}^{3} a_i \, E_{MOD,x}^{i} \quad (8)$$

The values of the fitting parameters a_i are reported in Table 1.

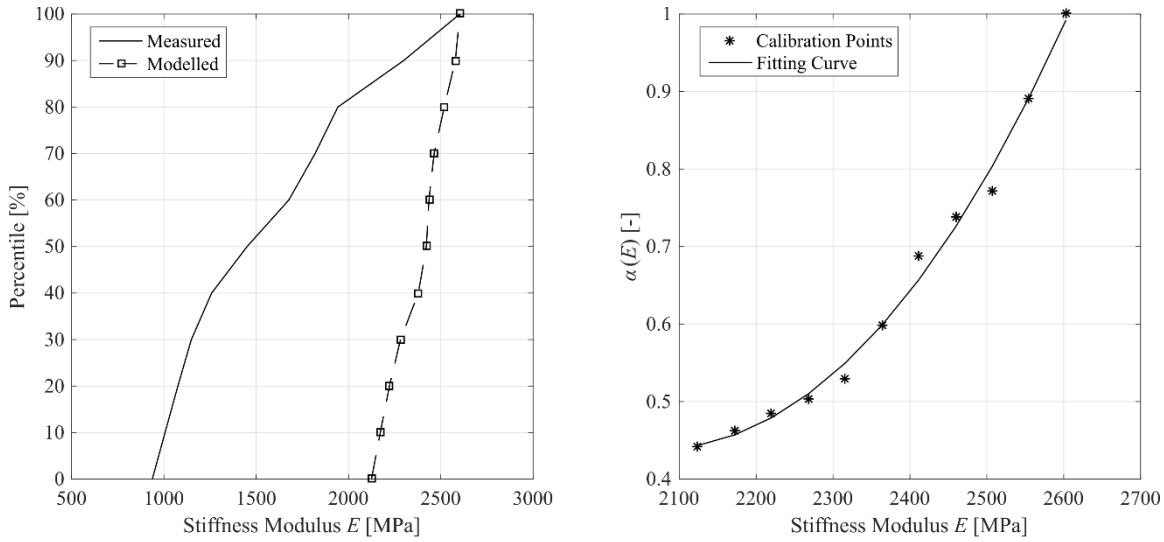

(a) (b)

Fig. 4. (a) Percentile analysis of measured (solid line) and modelled (dashed line with square markers) stiffness moduli; (b) fitting function $\alpha(E_{MOD,x})$ expressed by Eq. (8).

Table 1 – Fitting parameters a_i in Eq. (8).

a_0	a_1	a_2	a_3
-22.618	0.027	-1.24×10^{-6}	1.74×10^{-9}

The adjusted modelled trend of stiffness modulus is therefore derived working out the value of the fitting function $\alpha(E_{MOD,x})$ from Eq. (8) into Eq. (2). Figure 5 shows the comparison between trends of measured and (adjusted) modelled stiffness modulus along the calibration road stretch.

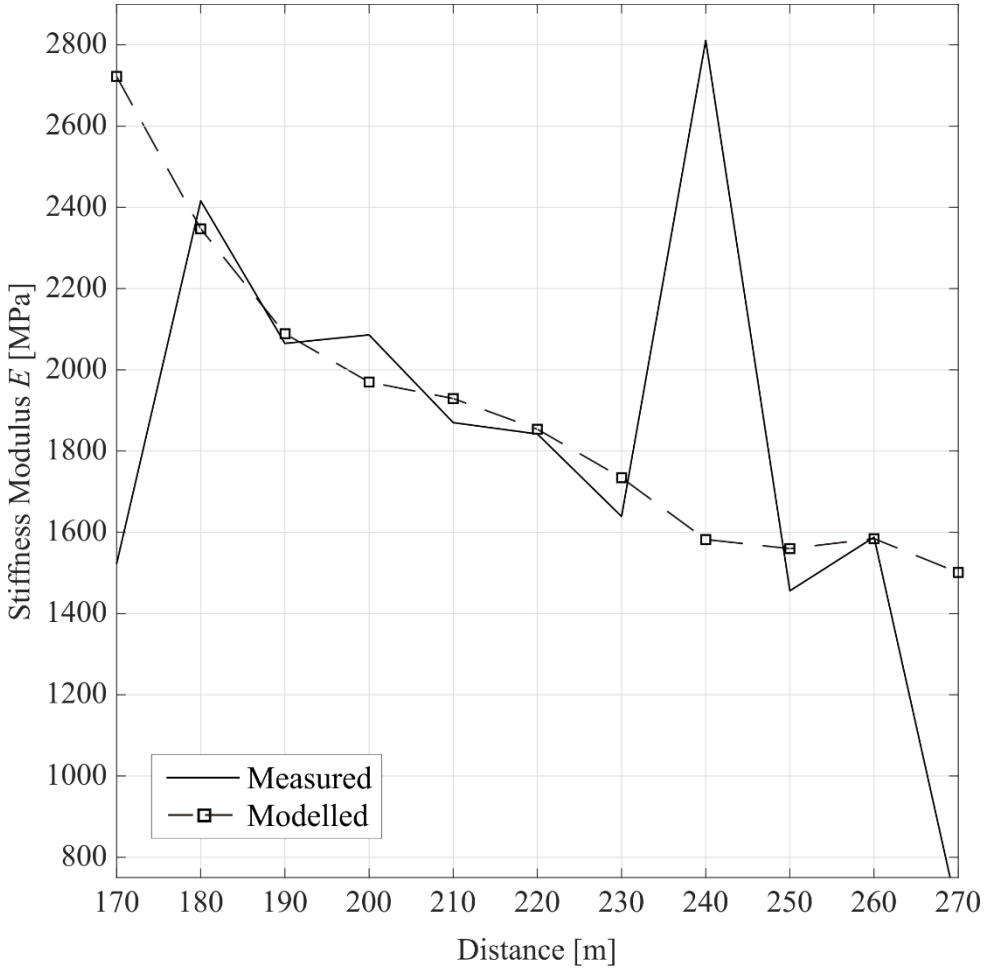

363

364 **Fig. 5.** Comparison between trends of measured (solid line) and modelled (dashed line with square
365 markers) stiffness modulus after the application of the fitting function $\alpha(E_{MOD,x})$ (Eq. (8)).

366

367 8. **RESULTS AND DISCUSSION**

368 **8.1. Validation of the quantitative model**

369 The trend of modelled values of fully-calibrated stiffness modulus $E'_{MOD,x}$ is estimated along the
370 processed road stretch length l_{tot}. An overall comparison between trends of measured and modelled
371 stiffness modulus is shown in Fig. 6. For the sake of clarity with the data interpretation, the 1200 m
372 road stretch length is divided into two sub-areas, i.e., from markers "0 m to 600 m" and "600 m to
373 1200 m". The area related to the calibration road stretch is marked in grey.

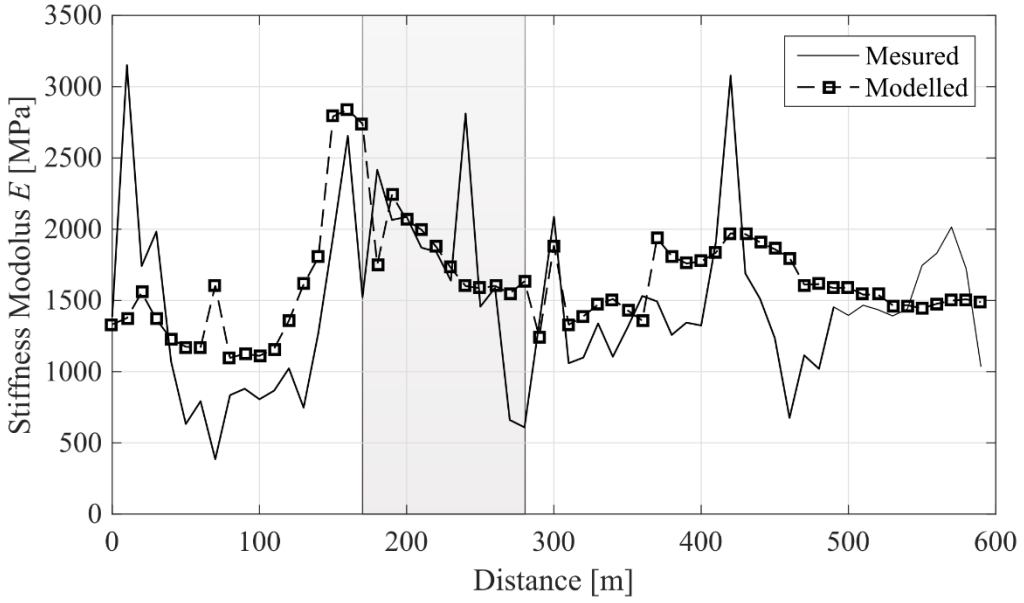

(a)

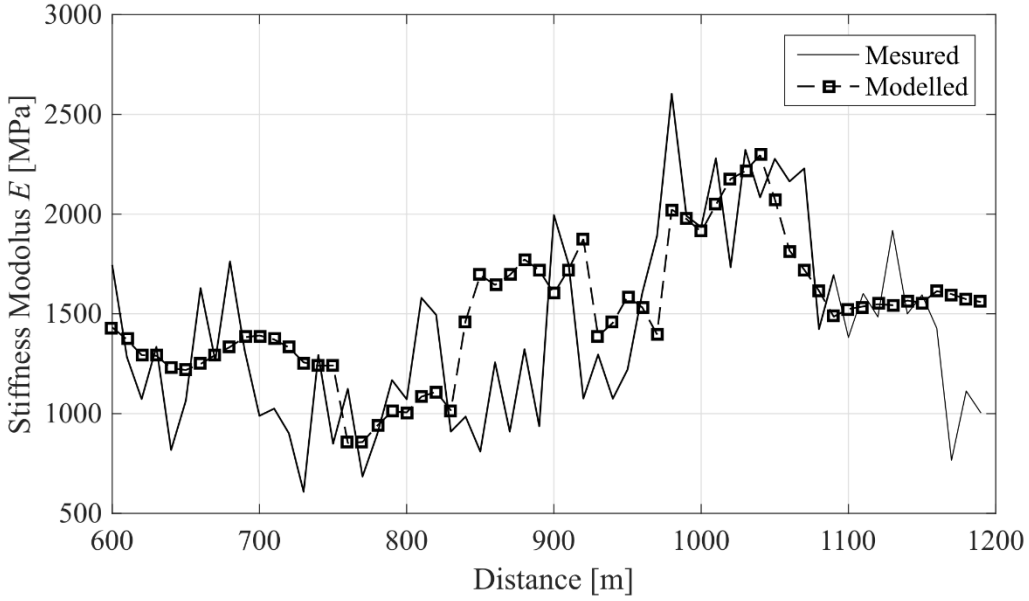

(b)

374

375

376 **Fig. 6.** Comparison between trends of measured $E_{MEA,x}$ (solid line) and modelled $E'_{MOD,x}$ (dashed line

377 with square markers) stiffness modulus after the application of the fully-calibrated model. The area

378 related to the calibration road stretch is marked in grey. (a) Markers "0 m – 600 m"; (b) markers "600

379 m – 1200 m".

380

A relatively good reliability of the model for the interpretation of the actual road pavement stiffness is proven. A few areas of ground-truth data misinterpretation from the model are still recognizable in the neighbourhood of markers “100 m”, “400 m”, “550 m” (Fig. 6(a)) and “900 m” (Fig. 6(b)). The normalised root-mean-square deviation (NRMSD) is equal to 0.273. This provides a quantitative measurement of disagreement between measured and modelled datasets of stiffness modulus.

The assumption made on the percentage size of the LFWD calibration points (i.e., ~10% of the data from the full dataset) is further investigated to verify the robustness of the model. To this purpose, the fully-calibrated model is applied with calibration data ranges comprised between 10% and 30% in steps of 5%; hence the relative values of NRMSD are found and plotted (Fig. (7)).

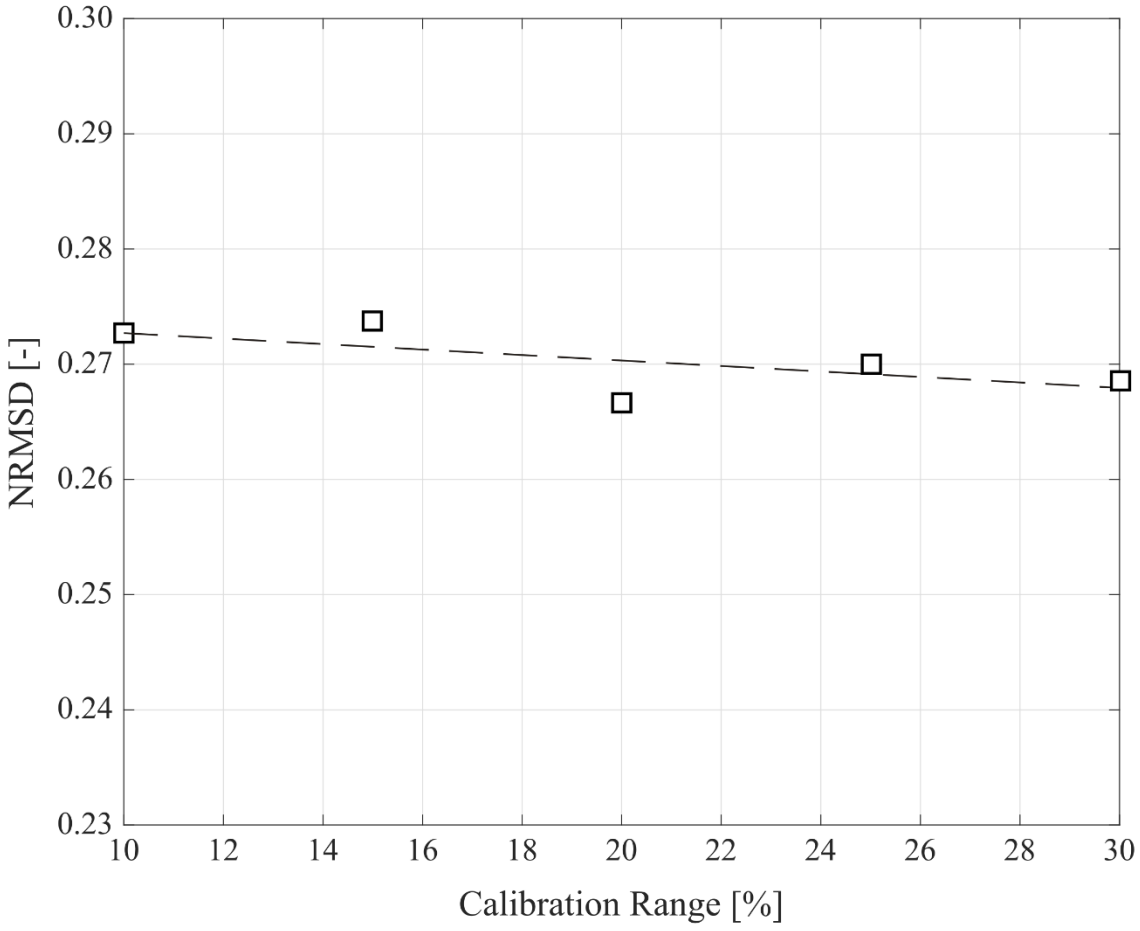

Fig. 7. The trend of NRMSD values of the model against the percentage range “10% - 30%” of LFWD calibration points.

393 It is worth noting how the robustness of the model has a weak dependence on the percentage range
394 of calibration points. This is proved by the slight variability of the NRMSD values and the fair
395 horizontality of the least square fitting trend line. Thereby, it is possible to argue that a robust
396 calibration can be performed using ~10% of ground-truth calibration points, whereas the length of
397 the relative full dataset is at least the same as the length of the road stretch investigated in this study.
398 This may represent an invaluable outcome for the development of a more time-efficient methodology
399 for the estimation of the stiffness of road flexible pavements. In fact, the use of FWD could be
400 potentially limited to the ~10% only of the full length of the roadway whereas the rest of the survey
401 could be carried out using an air-coupled GPR system for a more time-efficient data collection.
402
403 **8.2 Qualitative modelling of road pavement stiffness**
404 To foster the viability of using air-coupled GPR antenna systems in combination with FWD systems
405 in PMSs, a qualitative and streamlined approach to estimate stiffness of road flexible pavements is
406 further proposed. The rationale behind this process is to provide rapid identification of early decay
407 and loss of bearing capacity areas at the network level. Hence, time and cost of further and more
408 detailed investigations can be planned and allocated more effectively.

409 Stiffness moduli estimated from Eq. (1) and Eq. (2) are here considered as ground-truth and modelled
410 values, respectively. The investigated road stretch is divided into 50m-long value ranges of stiffness
411 modulus wherein the average value is taken as a benchmark. Three classes of stiffness are therefore
412 identified, i.e., “high stiffness”, “medium stiffness” and “low stiffness” classes. These are set as a
413 function of two thresholds, arbitrarily fixed at 1900 MPa and 1100 MPa, according to the overall
414 trend of modelled stiffness moduli. This step allows for customisation of the methodology as per the
415 specific requirements of the survey. Fig. (8) shows the outcomes of the qualitative modelling.
416

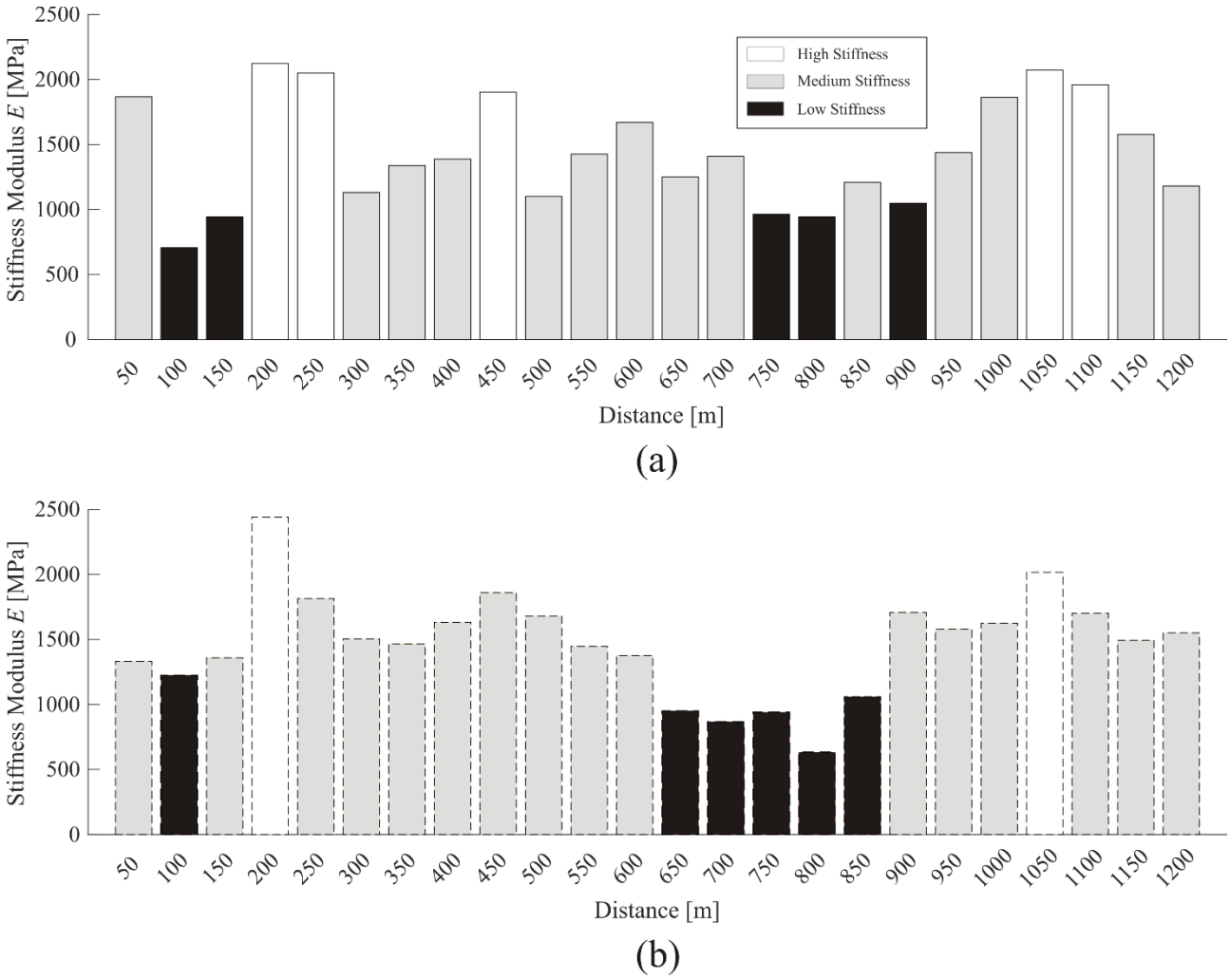

Fig. 8. Comparison between the three qualitative classes of stiffness modulus: (a) measured stiffness modulus (bar charts with solid contour lines); (b) modelled stiffness modulus (bar charts with dashed contour lines).

From the comparison between measured and modelled stiffness by the qualitative approach, matches of two main areas of lowest stiffness are observed in the value ranges "100 m – 150 m" and 700 m – 900 m". In addition, a good match between highest stiffness moduli is noticed in the value ranges "200 m – 250 m" and "1050 m – 1100 m". The remaining intervals match well with intermediate stiffness conditions of the road pavement.

It is worth noting the relative range of applicability of the proposed approach. The set values of the threshold are specific to the dataset collected in this investigation. Hence, they may change for a

different dataset (e.g., the same pavement structure at a different life cycle stage or another road pavement with a different cross section and/or construction materials). To this effect, the proposed methodology is reliable and can be used to investigate other road flexible pavements only if suitable threshold values are set after a preliminary data analysis at the network level.

9. CONCLUSION AND FUTURE PROSPECTS

This work proposes an experimental-based model for the assessment of stiffness in a road flexible pavement using ground-penetrating radar (GPR) and light falling weight deflectometer (LFWD). The model uses ground-truth data of road stiffness inferred from LFWD as well as geometric and physical information of the pavement structure derived from a GPR system equipped with a 2 GHz horn antenna.

To this purpose, 1500 m of a two-lane highway (one lane per direction) with a flexible pavement structure are investigated. After filtering out the outliers from the collected LFWD data (and the relative GPR traces), the model is calibrated via an optimisation process using the ground-truth stiffness moduli at the investigation points of a randomly-selected 100m-long road stretch (i.e., ~10% of the processed dataset), the thickness of the base layer and the central-peak amplitudes of the frequency spectrum. These latter parameters are both estimated using GPR and account for the structural quality of the pavement and the clay content in the load-bearing layers, respectively.

In addition to the quantitative approach for the estimation of the pavement stiffness modulus, a qualitative procedure is further developed. The investigated road stretch is divided into 50m-long value ranges of stiffness modulus, wherein the average value is taken as a benchmark. Three classes of pavement stiffness (i.e., “high stiffness”, “medium stiffness” and “low stiffness”) are therefore set based on two arbitrarily-fixed threshold values. These are selected according to the overall trend of modelled stiffness moduli and allow for customisation of the methodology as per the specific requirements of the survey.

The model viability is finally evaluated by quantitative and qualitative comparison of measured and modelled stiffness moduli. The quantitative analysis of the outputs shows a value of the normalised root-mean-square deviation (NRMSD) equal to 0.273. Hence, a relatively good agreement between measured and modelled data is proven. This outcome is also confirmed by the quantitative analysis, whereby good matches of the defined stiffness classes are found across the whole investigated road stretch.

It is important to emphasize the importance of the proposed methodology for extensive and time-efficient assessment of roads at the network level and potential implementation in pavement management systems (PMS). This could be crucial for road administrators and agencies in order to define priorities of intervention, allocate costs effectively and decrease the likelihood of envisaged accidents.

Future research could task itself with enriching the database for the development of the proposed methodology with a larger data sample from different road sections. In addition, different sources of ground-truth data for collection of stiffness moduli (e.g. falling weight deflectometer, curviameter, traffic speed deflectometer) could be used for the investigation of deeper domains and/or the gathering of more dense data. Comparison of model outputs against the actual strength and deformation data would allow for the understanding of the viability of different ground-truth equipment for modelling purposes.

Acknowledgements

The authors express their thanks to Mr. Spartaco Cera, from Roma Tre University, for technical assistance during the survey. Special thanks to IDS Georadar for supplying the GPR antenna system. This work has also benefited from the network activities carried out within the EU funded COST Action TU1208 “Civil Engineering Applications of Ground Penetrating Radar.”

References

1. S.–P. Miaou, The relationship between truck accidents and geometric design of road sections: Poisson versus negative binomial regressions, Accident Anal. Prev. 26 (4) (1994) 471–482.
2. P.C. Anastatoupulos, A.P. Tarko, F.L. Mannering, Tobit analysis of vehicle accident rates on interstate highways, Accident Anal. Prev. 40 (2) (2008) 768–775.
3. S. Tighe, N. Li, L.C. Falls, R. Haas, Incorporating road safety into pavement management, Transp. Res. Rec. 1699 (2000) 1–10.
4. ASTM D1195/D1195M-09, Standard test method for repetitive static plate load tests of soils and flexible pavement components, for use in evaluation and design of airport and highway pavements, ASTM International, West Conshohocken, PA., 2009.
5. ASTM D4695-03, Standard Guide for General Pavement Deflection Measurements, ASTM International, West Conshohocken, PA, 2008.
6. ASTM D4429-09a, Standard Test Method for CBR (California Bearing Ratio) of Soils in Place", ASTM International, West Conshohocken, PA, 2009.
7. ASTM D4694-09, Standard Test Method for Deflections with a Falling- Weight-Type Impulse Load Device", ASTM International, West Conshohocken, PA., 2009.
8. ASTM E2583-07, Standard Test Method for Measuring Deflections with a Light Weight Deflectometer (LWD)", ASTM International, West Conshohocken, PA., 2011.
9. A. Benedetto, F. Tosti, L. Di Domenico, Elliptic model for prediction of deflections induced by a Light Falling Weight Deflectometer. J. Terramechanics 49 (1) (2012) 1–12.
10. P.R. Fleming, M.W. Frost, J.P. Lambert, Review of lightweight deflectometer for routine in situ assessment of pavement material stiffness, Transp. Res. Rec., (2007) 80–87
11. A. Benedetto, L. Pajewski, Eds. (2015), Civil Engineering Applications of Ground Penetrating Radar, Springer - Book Series: Springer Transactions in Civil and Environmental Engineering; doi: 10.1007/978-3-319-04813-0
12. J.-M. Simonin, J.-L. Geffard, P. Hornych, Performance of deflection measurement equipment and data interpretation in France, International Symposium Non-Destructive Testing in Civil

Engineering (NDT-CE) September 15–17, 2015, Berlin, Germany.

13. A. Zofka, J. Sudyka, Traffic speed deflectometer (TSD) measurements for pavement evaluation, in Proc. of the International Symposium on Non-Destructive Testing in Civil Engineering (NDT-CE), Berlin, Germany, Sept. 15–17, 2015.

14. A. Zofka, M. Graczyk, J. Rafa, Qualitative evaluation of stochastic factors affecting the Traffic Speed Deflectometer results, in Proc. of the Transportation Research Board 94th Annual Meeting, Washington DC, USA, Jan. 11–15, 2015.

15. C. Bruschini, B. Gros, F. Guerne, P.-Y. Pièce, O. Carmona, Ground penetrating radar and imaging metal detector for antipersonnel mine detection, J. Appl. Geophys. 40 (1-3) (1998) 59–71.

16. D. Goodman, Ground-penetrating radar simulation in engineering and archaeology, Geophysics, 59 (2), (1994) 224–232.

17. A.K. Benson, Applications of ground penetrating radar in assessing some geological hazards: examples of groundwater contamination, faults, cavities, J. Appl. Geophys. 33 (1-3) (1992) 177–193.

18. L.A. Plewes, B. Hubbard A review of the use of radio-echo sounding in glaciology, Progress in Physical Geography, 25 (2) (2001) 203–236.

19. F. Tosti, S. Adabi, L. Pajewski, G. Schettini, A. Benedetto, Large-scale analysis of dielectric and mechanical properties of pavement using GPR and LFWD, in Proc. of the 15th International Conference on Ground Penetrating Radar, Brussels, Belgium, Jun.-July 2014, pp. 868–873.

20. D.J. Daniels, Ground Penetrating Radar, IEEE Radar, Sonar, Navigation and Avionics Ed., 2006.

21. D.G. Fredlung, H. Rahardjo, M.D. Fredlung, Unsaturated Soil Mechanics in Engineering Practice, Jhon Wiley & Sons Ed., 2012.

22. J.K. Mitchell, Fundamentals of Soil Behaviour, Second Edition. John Wiley & Sons Ed.,

1993.

23. S.H. Carpenter, R.L. Lytton, J.A. Epps, Pavement cracking in west texas due to freeze-thaw cycling, Transp. Res. Rec., 532 (1975) 1–13.

24. T. Scullion, T. Saarenketo, Using suction and dielectric measurements as performance indicators for aggregate base materials, Transp. Res. Rec., 1577 (1997) 37–44.

25. T. Saarenketo, The use of dielectric and electrical conductivity measurements and ground penetrating radar for frost susceptibilty evaluations of subgrade soils, in Proc. of the Symposium on the Application of Geophysics to Engineering and Environmental Problems (SAGEEP) 95, 1995, pp. 73–85.

26. A. S. Noureldin, K. Zhu, S. Li, D. Harris, Network pavement evaluation using falling weight deflectometer and ground penetrating radar, Transp. Res. Rec., 1860 (1) 765–797.

27. Y.H. Huang, Pavement Analysis and Design, Prentice-Hall Ed., 2004.

28. E. Tutumler, D.S. Little, S.-H. Kim, A validated model for predicting field performance of aggregate base courses, in Proc. of the 82nd Annual Meeting of the Transportation Research Board, Washington, DC, 2003.

29. R. Horn, Strength of structured soils due to loading- a review of the processes on macro- and microscale-European aspects. In: Larson WE, Blake GR, Allmaras RR, Voorhees WB, Gupta S, editors. Mechanics and related processes in structured agricultural soils. Kluwer Publ; Applied Sciences; 1989. pp. 9–22.

30. D.M. Burmister, The general theory of stresses and displacements in layered systems, J. Appl. Phys., 16, 126 (1945) (2004).

31. C.R. Foster, R.G. Ahlvin, Stresses and deflections induced by a uniform circular load, in Proc. of Highway Research Board, 33 (1954) 467–470.

32. M. Novak, B. Birgisson, R. Roque, Near-surface stress states in flexible pavements using measured radial tire contact stresses and ADINA, Comput. Struct., 81 (2003) 859–870.

33. S. Oteng-Seifah, P. G. Manke, Study of Rutting in Flexible Highway Pavements in Oklahoma

(Abridgment), Transp. Res. Record, 602 (1976) 97–99.

34. A.L. Simpson, J.F. Daleiden, W.O. Hadley (1995) Rutting Analysis from a Different Perspective, Transp. Res. Rec., 1473, 9-17.

35. C. Plati, A. Loizos, Estimation of in-situ density and moisture content in HMA pavements based on GPR trace reflection amplitude using different frequencies, J. Appl. Geophys., 97 (2013) 3–10.

36. F. Tosti, C. Patriarca, E. Slob, A. Benedetto, S. Lambot, Clay content evaluation in soils through GPR signal processing, J. Appl. Geophys., 97 (2013) 69-80.

37. F. Tosti, A. Benedetto, L. Bianchini Ciampoli, S. Lambot, C. Patriarca, E. Slob, GPR analysis of clayey soil behaviour in unsaturated conditions for pavement engineering and geoscience applications, Near Surf. Geophys., 14(2) (2016) 127-144.

38. H. Jol (Ed.), Ground Penetrating Radar, Elsevier, 2009.

39. P. Ullidtz (Ed.), Pavement Analysis, Elsevier, 1987.

40. S. Baltzer, J.M. Jansen, Temperature correction of asphalt-moduli for FWD measurements, in Proc. of the 4th International Conference on the Bearing Capacity of Roads and Airfields (BCRRA), University of Minneapolis, Minnesota, July 17 -21, 1994, pp. 7–25.

41. A. Benedetto, F. Tosti, L. Bianchini Ciampoli, F. D'Amico, An overview of ground-penetrating radar signal processing techniques for road inspections, Signal Process., 132 (2016) 201–209.

42. I.L. Al-Qadi, S. Lahouar, Measuring layer thicknesses with GPR – Theory to practice, Constr. Build. Mater., 19 (2005) 763–772.

43. ISPRA – Istituto Superiore per la Protezione e la Ricerca Ambientale - http://sgi.isprambiente.it/geoportal/catalog/sgilink/map100k.page (retrieved 22 Jun. 2017).